Analytical Methods

Accepted Manuscript

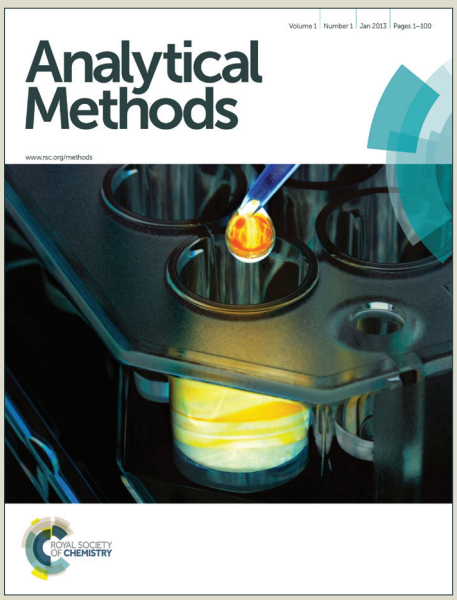

ROYAL SOCIETY OF CHEMISTRY

www.rsc.org/methods

Mesoporous silica particles embedded functional graphene oxide as an efficient platform for urea biosensing

Graphical Abstract

Mesoporous silica particles embedded graphene oxide (GO) hybrid system is a promising platform for electrochemical biosensing owing to its large 2-dimensional structure, fast electron transfer kinetics, improved hydrophilic nature and surplus functional groups. Here, GO sheets were synthesized by Hummer's improved method and sub-micron sized homogeneous mesoporous silica (SiO_2) particles were prepared by Stober's method. The SiO_2 particles have been embedded on the GO surfaces and have optimized with different concentrations for better applicability and hydrophilicity. Micro-structural and spectroscopic characterization of as-synthesized materials has been carried out to confirm the successful synthesis as well as the functionalities required for biosensing. Scanning electron microscopy investigations suggest that the average size of the SiO_2 particles decorated on the GO surface is ~500 nm. Raman investigation provides information regarding the increase in defects and disorder on GO surface with the increase in SiO_2 content. The optimized GO- SiO_2 (GOS) composite electrode has been prepared by the electrophoretic deposition technique and has been used for the attachment of urease and glutamate dehydrogenase enzymes for urea detection employing cyclic voltammetry method. The reproducibility, specificity and stability of the fabricated biosensor found to be excellent for the urea sensing. Such an easy and cost effective material based GOS urea sensor showed high sensitivity (2.6 μA/mM/cm^2) and a good detection limit (14 mg/dL).

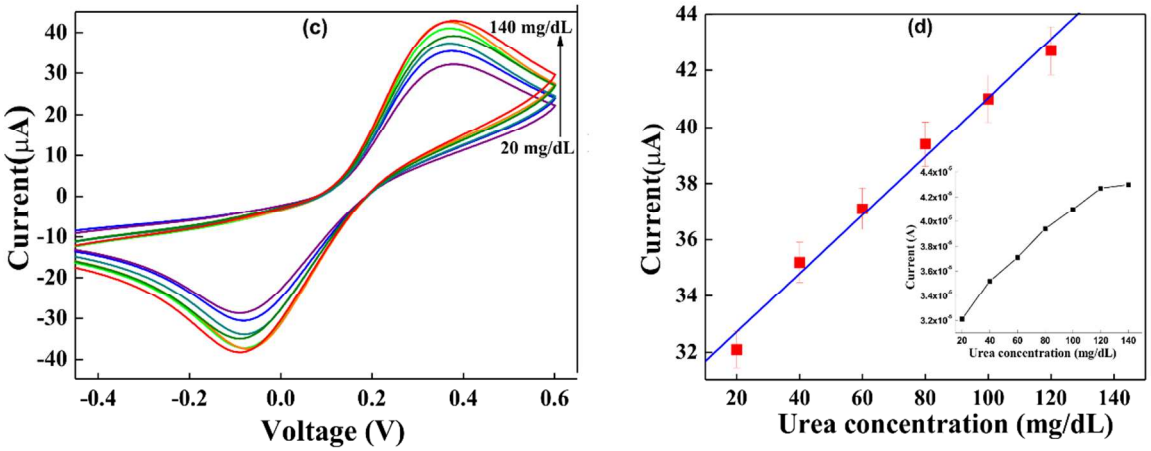

Mesoporous silica particles embedded functional graphene oxide as an efficient platform for urea biosensing

Shiju Abraham,[†,‡] Valerian Ciobota,[‡] Saurabh Srivastava,[†,§] Sunil K. Srivastava,[£] Rajesh K. Singh,[¥] Jan Dellith,[€] B. D. Malhotra,[¢] Michael Schmitt,[‡] Jürgen Popp,[,‡] Anchal Srivastava[†,*]*

[†]Department of Physics, Banaras Hindu University, Varanasi, 221005, India

[‡]Institute of Physical Chemistry, Friedrich-Schiller-University Jena, Helmholtzweg 4, D-07743 Jena, Germany

[§]Department of Science and Technology Centre on Biomolecular Electronics, Biomedical Instrumentation Section, National Physical Laboratory, New Delhi 110012, India

[£]Department of Pure and Applied Physics, Guru Ghasidas University, Main Campus, Koni, Bilaspur- 495009, India

[¥]Department of Applied Physics, Indian Institute of Technology (B. H. U.), Varanasi, 221005, India

[€]Institute of Photonics Technology, Albert-Einstein-Str. 9, D-07445, Germany

[¢]Department of Biotechnology, Delhi Technological University, Delhi 11042, India

***Corresponding Author**

[*]E-mail: anchalbhu@gmail.com (Dr. Anchal Srivastava)

Phone No.: +91-9453203122, Fax: +91-542 2368174

Abstract

Mesoporous silica particles embedded graphene oxide (GO) hybrid system is a promising platform for electrochemical biosensing owing to its large 2-dimensional structure, fast electron transfer kinetics, improved hydrophilic nature and surplus functional groups. Here, GO sheets were synthesized by Hummer's improved method and sub-micron sized homogeneous mesoporous silica (SiO_2) particles were prepared by Stober's method. The SiO_2 particles have been embedded on the GO surfaces and have optimized with different concentrations for better applicability and hydrophilicity. Micro-structural and spectroscopic characterization of as-synthesized materials has been carried out to confirm the successful synthesis as well as the functionalities required for biosensing. Scanning electron microscopy investigations suggest that the average size of the SiO_2 particles decorated on the GO surface is ~500 nm. Raman investigation provides information regarding the increase in defects and disorder on GO surface

with the increase in SiO_2 content. The optimized GO- SiO_2 (GOS) composite electrode has been prepared by the electrophoretic deposition technique and has been used for the attachment of urease and glutamate dehydrogenase enzymes for urea detection employing cyclic voltammetry method. The reproducibility, specificity and stability of the fabricated biosensor found to be excellent for the urea sensing. Such an easy and cost effective material based GOS urea sensor showed high sensitivity (2.6 μA/mM/cm^2) and a good detection limit (14 mg/dL).

Introduction

The estimation of urea in serum, blood and urine is very important for the diagnosis of renal and liver diseases. An increase in urea level (normal range in blood is 15–40 mg/dL) causes renal failure, urinary tract obstruction, dehydration, shock, burns, and gastrointestinal bleeding, etc. Development of sensitive, selective, reliable and low cost material based biosensor is of great importance for the diagnosis and management of urea. In recent years nanomaterials based electrochemical biosensors have attracted wide popularity and applicability due to their good selectivity, portability, inexpensiveness and simplicity. The two-dimensional (2D) nanomaterials, graphene and its derivative- graphene oxide (GO) have been attracted significant attention of researchers from various disciplines in the last decade after the successful isolation of a single layer of graphite on an insulating silica (SiO_2) substrate[1-4]. Apart from graphene, there has been a great upsurge of interest towards studying GO, a heavily oxygenated graphene derivative[5]. These materials are now in the forefront of attention as a novel cousin of graphene[6-9]. The excellent solubility, stability against aggregation, large surface area, etc. of GO have led to many interesting applications, such as electrochemical sensing, electro catalysis and immunoassays etc[10-12]. Further, since most of the atoms of the GO sheet are exposed to the surface, slight changes in the local charge environment due to the adsorption of biomolecules provide significant changes in their electrical properties[13]. This will be more pronounced when biocompatible, porous particles are embedded on the GO surfaces. These interesting properties by the synergetic effects may perhaps be utilized in the fabrication of more sensitive and selective biosensors.

In view of the special characteristics of GO, several nanoparticles (NPs) (such as SiO_2, Au, Ag, Pt, Ti etc.)[14-18] have been introduced onto the surface of GO and thereby giving rise to novel nano-hybrid materials with unique properties and intriguing applications. SiO_2, a typical non-metallic oxide, is of special interest due to its widespread use as a cost-effective material in the construction of super hydrophilic/super hydrophobic surfaces. Among the various oxide NPs, it has been found that, the control of size as well as porosity in SiO_2 particles is comparatively easy. The well-defined surface properties of SiO_2 particles are beneficial for site-specific delivery of different functional molecules of various sizes and shapes[19]. The high porosity of SiO_2 particles, which results in large surface area available for the encapsulation as well as for the immobilization of various sensing molecules leading to fast response time and low detection limit[20,21]. SiO_2 dispersion play a major role in several applications like catalysts, membranes, biocompatible solid support, etc. [22,23]. Further it have found to be a suitable candidate for many biological applications owing to its good biocompatibility, enhanced electrochemical properties and excellent

enzymatic activity in their respective enzyme reactions[20,24,25]. While considering the composite formulation and studies; silver NPs/ functionalized SiO_2/ GO composite is demonstrated to be a potential candidate for biosensing in glucose detection[26]. According to Watcherotone *et al*.[27], graphene-silica composite thin films have several potential applications owing to its conducting and transparent property. Kou and Gao[28] synthesized SiO_2 NPs – covered GO hybrids and showed that GO-SiO_2 hybrids exhibit excellent hydrophilic nature and can be used as a building block to construct large area super hydrophilic surfaces. Liu *et al*[29].studied the surface assembly of GO nanosheets on SiO_2 particles, and used this composite for the selective isolation of hemoglobin. Considering the above studies, the GOS composite system is of much interest because of its high solubility in water, easy synthesis, bulk production and abundant functional groups. The biocompatible, stable and porous SiO_2 particles combine with the compatible properties of GO, making the hybrid system (GOS) well suited for many applications, especially in biosensing where the composite haven't explored well.

While keeping all the above factors in mind, the work presented in the following report is about the synthesis and fabrication of thin film of GOS composite onto an indium tin oxide (ITO) glass substrate by electrophoretic deposition (EPD) technique. These thin films have been further used to immobilize urease (Urs) and glutamate dehydrogenase (GLDH) for urea detection by cyclic voltammetry (CV) technique. The fabricated bioelectrode showed good stability, specificity as well as reproducibility. This GOS based urea sensor shows high sensitivity (2.6 $\mu A/mM/cm^2$) and good detection limit (14 mg/dL) comparing to many other reports.

Experimental

Chemicals

Tetra ethyl ortho-silicate (TEOS, Aldrich, purity ≥ 99% with trace metal basis), graphite flakes (NGS Naturgraphit GmbH, Germany), ammonia solution, ethanol, H_2SO_4, H_3PO_4, $KMnO_4$, H_2O_2, etc. used were of analytical reagent grade. All the chemicals employed for the fabrication of the urea biosensor, namely, Urs, GLDH, nicotinamide adenine dinucleotide (NADH) and α-ketoglutarate (α -KG), were procured from Sigma-Aldrich.

Synthesis of GO and SiO_2 particles

Few years ago, an improved method for producing GO has been proposed by Marcano *et al*.[30]. This method has some distinct advantageous features over the Hummers´ method[6] in the sense that it yields a higher fraction of hydrophilic carbon material. In the improved synthesis of GO, a 9: 1 combination of concentrated H_2SO_4 / H_3PO_4, (120ml /13.33ml) is added to 1g of graphite flakes and 6 g of $KMnO_4$. The above mixing process creates slight exothermic reaction, and the mixture is stirred for 12 h keeping a constant temperature of 50°C. The reaction is subsequently quenched by adding ~135 ml of ice with 30% H_2O_2. This mixture is then shifted, centrifuged and filtered. The solid material thus obtained (GO) is washed with 30% HCl and distilled water until pH ~7 is reached, then the material was dried. SiO_2 particles were synthesized by the well-known Stober's method[21]. Briefly, a 120 ml of ethanol (98%) is taken in a round-bottom flask and 24 ml of ammonia solution was added to it. This solution is kept for stirring and after 20 minutes, the sol gel reaction was initiated by adding 12 ml of TEOS. The stirring was continued for 10 h until the solution gradually turned white in colour. The above colloidal solution of SiO_2 particles were used to decorate the surface of GO. The remaining solution is centrifuged at the rate of 3000 rpm for 30

minutes. The solid material collected was washed with ethanol and then dried at 80°C. Final solid product obtained is used for further characterizations.

Production of GOS

The as synthesized GO was well dispersed (0.35mg/ml) in double distilled water by continuous ultra-sonication for an hour. The SiO_2 dispersion was prepared in ethanol at a concentration of 20 mg/ml. Four composite solutions were prepared by taking a constant amount of the above GO solution (25 ml each) and varying amounts of SiO_2 solution [250µL (~5mg), 500µL (~10mg), 750µL (~15mg) and 1000µL (~20mg)]. These composite solutions are abbreviated as GOS1, GOS2, GOS3 and GOS4 respectively. The mixture solution was then sonicated continuously for an hour by gradually increasing the temperature to 60ºC. The solution was then subsequently stirred for 4 h and centrifuged. Finally the solution was washed with ethanol, distilled water and then dried at 70ºC to get the solid product GOS. Among the four GOS composites, GOS3 found to be more hydrophilic in nature and showed good film forming capabilities.

Fabrication of GOS thin film electrodes

Thin films of nanostructured GOS over ITO electrodes are formed by the EPD technique. Here a 10 mL colloidal solution of GOS3 (3 $mgdL^{-1}$) in acetonitrile is given into a two-electrode glass cell. A platinum foil (1×2cm) is used as the counter electrode and a pre-cleaned ITO-coated glass substrate having a sheet resistance of 30 Ω as working electrode; both electrodes are separated by 1 cm. The film deposition is carried out onto the desired ITO-coated glass plate (0.25 cm^2) by applying a DC voltage of 120 V for 2 minutes. 10^{-5}–10^{-4} mol of Mg $(NO_3)_2.6H_2O$ is added into the colloidal suspension acting as an electrolyte and creating surface charge on the GOS3 desired for EPD. The two electrodes were placed parallel to each other and were dipped in the GOS3 colloidal suspension. The film is deposited onto the desired ITO-coated glass plate. The film is then removed from the suspension followed by washing with deionized water and drying.

Solution preparation and immobilization of enzyme

Urs (10 mg/mL) and GLDH (1 mg/dL) solutions were freshly prepared in the phosphate buffer (50 mM, pH~7.0). A stock solution of urea (200 mg/dL) was prepared in deionized water and is kept at 4 ˚C. This stock solution was used to get different concentrations of urea by further dilution. NADH (3.7 mg/dL), and α –KG (47.5 mg/dL) were freshly prepared in double distilled water. Further, 10 µL of bienzyme solution containing Urs (10 mg/mL) and GLDH (1 mg/mL) in a 1:1 ratio was covalently immobilized by uniformly spreading on the activated electrode surface and incubating it for about 12 h. The immobilization occurs through the surface adsorption as well as through the formation of amide bond between terminal COOH group of GO and terminal NH_2 group of the enzyme. The Urs-GLDH/GOS/ITO bioelectrode was then washed with PBS buffer and stored at 4 ˚C when not in use. This enzymatic electrode was utilized for urea detection using cyclic voltammetric (CV) technique.

Characterization

The structure of GO, SiO_2 and GOS composites were characterized by X-ray diffraction (XRD) technique (Rigakuminiflex-II diffractometer at 30 kV and 15mA) using Cu-Kα1 radiation (λ=1.5405 Å). The surface morphology of the samples prepared was investigated using scanning electron microscopy employing JEOL – Model JSM6300F-SEM. The molecular structure of the material was investigated using Fourier transform infrared

(FT-IR) spectroscopy (Perkin Elmer Spectrum 65, FT-IR spectrometer). Raman spectroscopic measurement was made by using two different Raman spectrometers. One by using a single monochromator (TRIAX 550, JobinYvon, France) with the 514.5 nm line from an Ar laser (Innova 308 Series, Coherent, USA) as a Raman excitation source. Another Raman spectrometer (HR LabRam inverse system, JobinYvon Horiba) with a Raman excitation source of wavelength 532 nm from a frequency doubled Nd: YAG laser was used. The electrochemical studies related to urea detection were carried out on Autolab Potentiostat/Galvanostat (Eco Chemie, Netherlands). The measurements was carried out using a three electrode cell with Urs-GLDH/GOS/ITO bioelectrode as the working electrode, platinum (Pt) as the counter electrode, and a Ag/AgCl electrode as a reference electrode in 50 mM phosphate buffer saline (PBS) of pH 7.0 containing 5 mM of $[Fe(CN)_6]^{3-/4-}$.

Results and discussion

Structural characterization

The XRD pattern of the three materials, namely GO, SiO_2 and GOS3 composite are presented in Figure 1.

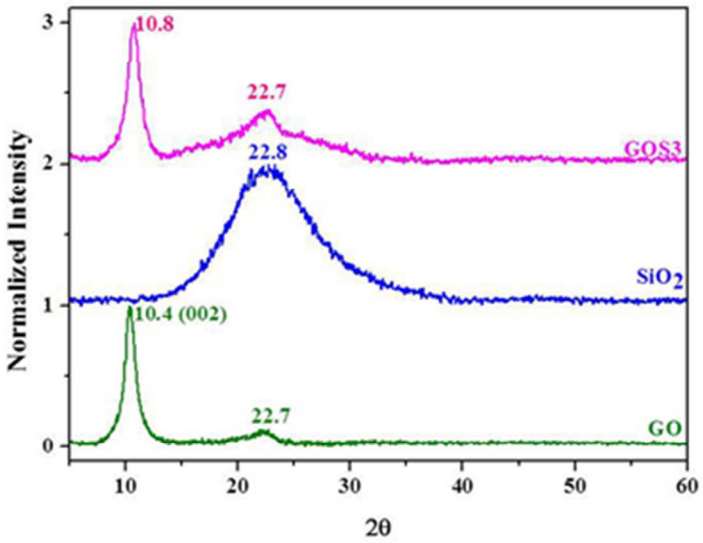

Figure 1. X-ray Diffraction (XRD) Patterns of: (a) GO sheets, (ii) SiO_2 particles, (iii) GOS3

The GO shows a peak at 10.4º (002) (corresponding to a d-spacing of 0.85 nm), which matches with the well-known XRD peak of GO[28]. GO also shows a weak broad peak at 22.7º, which has nearly one eighth of the integrated intensity of the main GO peak. This weak XRD peak interpreted in terms of short-range order in the stacked graphene like sheets[31]. The XRD pattern of SiO_2 particles that the peak centered at 22.8° (JCPDS File No. 47-1301) is relatively broad and is attributed to its more amorphous nature as well as its quite large particle size distribution [between 300 to 500 nm, as seen from the SEM micrograph shown in Figure 2(b)]. In the case of the composite

system, GOS3, the analyzed XRD pattern gives rise to two peaks at 10.8 (corresponding to a d-spacing of 0.82 nm) and 22.7º. The interlayer spacing decreases (from 0.85 to 0.82 nm), when GO transform to GOS.

SEM images of the GO, SiO_2 particles and their different composite systems are presented in Figures 2(a) to 2(f) reveal interesting features about their morphology and microstructure. The SEM micrograph shown in Figure 2(a) supports the formation of uniform GO sheet of different layers, with wrinkles marked by arrows. From Figure 2(b), it is evident that the size of the SiO_2 particles is ~500 nm and the distribution of the particle size is quite narrow. For any practical application, optimization of the concentration of SiO_2 particles on the GO sheet is required. This provides an opportunity to study the properties of GOS composite with varying concentration of SiO_2 particles. As the concentration of SiO_2 particles is varied from GOS1 to GOS4 (250 to 1000µl), the density of the SiO_2 particles decorated on the GO sheet increases, which is evident from Figures 2(c) to 2(f). Figure 2(f) shows the extreme case wherein SiO_2 particles are densely packed one above another. The porous nature of the silica particles is visible from Figure 2(f). The pore diameter vary approximately in a range of 2-6nm [by Brunauer-Emmett-Teller (BET) pore size analysis gives, an average pore diameter~5nm]. The porous nature enhances its surface area further and allows higher loading of biomolecules (enzymes) for the effective sensing of particular analyte. Here the pores work as a better substrate for maximum loading.

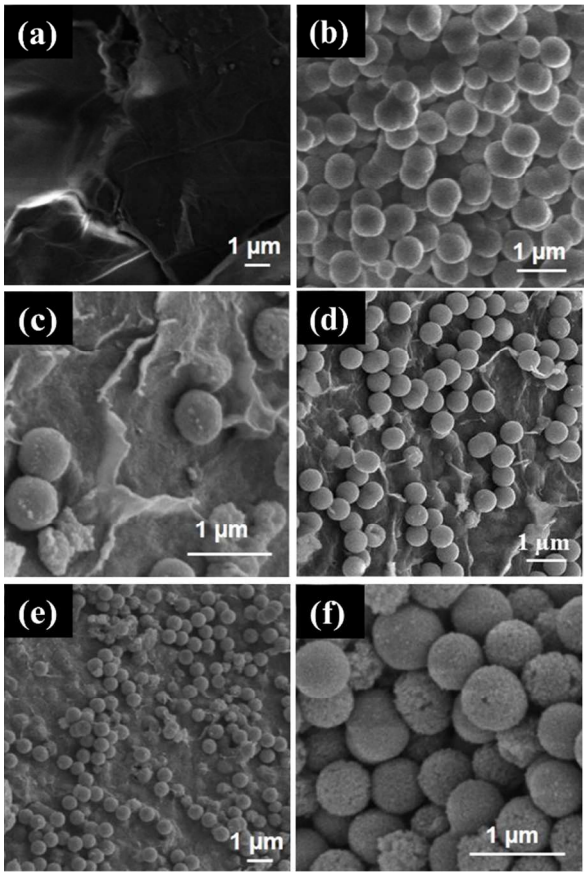

Figure 2. SEM micrograph of (a) GO synthesized by improved Hummer's method, (b) Stober's SiO_2 particles, (c-f) SiO_2 particles decorated GO with increasing concentration of SiO_2 content (c) GOS1, (d) GOS2, (e) GOS3, (f) GOS4.

Spectroscopic characterization

The FTIR spectra of GO, SiO_2 particles and the four GOS composites are presented in Figure 3(a). Figure 3(a) (i) shows the FTIR spectra of GO, which have different hydrophilic functional groups attached to graphene. A broad band extending from nearly 2800 to 4000 cm^{-1} appears in all the spectra [see spectra (i) to (vi) in Figure 3(a)] due to O–H stretching vibration from the different species. A weak band at 2928 cm^{-1} observed in the IR spectra of GO [Figure 3a (i)] attributed to the C-H stretching mode of the carboxylic group. A band at 1110 cm^{-1} observed in GO corresponds to the C–O stretching vibration of the alkoxide group and the C–O stretching vibration due to carboxylic group is observed at ~ 1400 cm^{-1}. An interesting feature of this study is that the intensity of the IR band arising due to the presence of carboxylic functional group decreases as the concentration of SiO_2 increases. However, this decrease is accompanied by a simultaneous significant increase in the relative intensity of the IR band at ~ 1100 cm^{-1} corresponding to the C–O stretching vibration of the alkoxide group. It is worth mentioning that the carboxylic C–O stretching and the alkoxy C-O stretching vibrations which appear in the IR spectra are essentially due to the different functional groups situated at the edges of the GO sheet. Besides this, the spectra of the different GOS composites also shows a prominent band at 1632 cm^{-1} which has been attributed to scissor type O-H bending vibration of molecular H_2O. The intensity of this band is largest in the case of GO and shows a decreasing trend for increasing SiO_2 concentration. The broad peak around 1725 cm^{-1} represents the stretching vibration of C=O bond of the carboxylic acid group. The three IR peaks, which appear in Figure 3(a) (vi) below 1100 cm^{-1}, are the characteristic peaks of the Si-O-Si bonds. The most intense of these three peaks, which also appears at the highest wavenumber position at ~ 1070 cm^{-1} corresponds to the anti-symmetric Si-O-Si stretching vibration (TO_3 mode)[32]. The second IR band observed at 953 cm^{-1}, can be assigned to the Si-OH stretching vibration[33]. The third IR peak at 803 cm^{-1} was assigned to the Si-O-Si symmetric stretching (TO_2 mode) vibration. These characteristic functional groups of GO and SiO_2 are beneficial for their nice binding and also for the immobilization of enzyme. The Raman spectra of SiO_2 have been recorded using 532 nm excitation (see lower frame of Figure 3(a)). Two prominent Raman bands at ~ 800 and ~ 970 cm^{-1} are observed, which match nicely with the IR absorption bands for the Si-O-Si symmetric stretching and Si-OH stretching vibrations, respectively. The Raman measurement was basically done to compare the IR and Raman wavenumber of the vibrational modes of SiO_2 alone. These peaks are well resolved and appear with sufficient intensity in the IR as well as Raman spectra of SiO_2, whereas in the IR spectra of the composite having different concentration of SiO_2, Si-OH stretching band appears with a very feeble intensity which diminishes drastically for decreasing SiO_2 concentration.

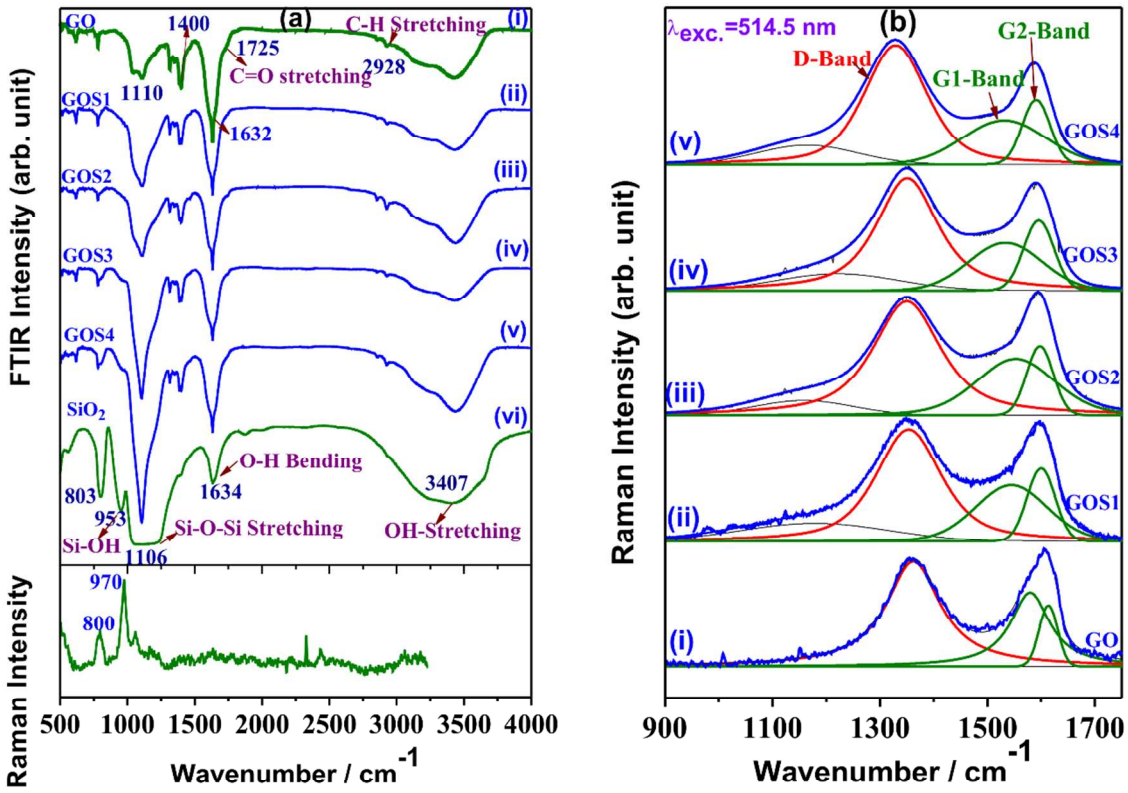

Figure 3(a). FTIR spectrum of (i) GO, (ii) GOS1, (iii) GOS2, (iv) GOS3, (v) GOS4, (vi) SiO_2 particles and in the lower frame: Raman spectra of SiO_2 particles excited by 532 nm. **Figure 3(b).** Raman spectra of (i) GO, (ii) GOS1, (iii) GOS2, (iv) GOS3 and (v) GOS4 showing the component bands D, G1 and G2

Raman spectroscopy is very well suited to distinguish between sp^2 and sp^3 hybridization in carbonaceous materials[34,35]. The two main characteristic Raman bands observed in almost all carbon-based materials are the G-band and D-band. The G peak only disperses in more disordered carbon, where the dispersion is proportional to the degree of disorder. Kudin *et al.*[34] observed and reported the broadening of the G band in functionalized graphene sheet and GO. The D-band (disorder-induced band) around 1350 cm^{-1} in the defected graphite originates from the one-phonon second order Raman scattering process. The Raman spectra of GO and GOS composites were excited with 514 nm laser are shown in Figure 3(b) (i-v).

Table 1. Peak position of the D and G (G1 and G2) Raman bands and I_D/I_G (by area) of GO and GOS composite measured using 514.5nm excitation wavelength.

Name of the sample	Peak position at 514.5 nm excitation wavelength			I_D/I_G
	D	G1	G2	
GO	1362	1580	1614	1.19
GOS1	1353	1545	1600	1.34
GOS2	1350	1553	1598	1.67
GOS3	1350	1534	1596	2.20

Raman spectra were fitted to three component bands namely D, G1 and G2 bands by using *SpectraCalc* software and the results are presented in Table 1. In *Spectra Calc* analysis, the guess values for the peak positions and line widths of the stipulated Raman bands are given as input. A non-linear least square fit assumes an appropriate intensity for each peak and the measured Raman profile is fitted (using a mixture of Lorentzian/ Gaussian) to get the peak position, linewidth and intensity of all the peaks. The analysis of the Raman spectra of GOS4 is missing in Table 1 as the GO surface is fully covered with SiO_2 particles [evident from SEM image 2(f)]. The G-band, which is the characteristic vibration of the sp^2 carbon in most of the carbon-based materials, is split into two components, G1 and G2. In a study[2] on functionalized multilayered graphene (MLG), it has been pointed out that the splitting of the G band probably result from the presence of functional groups, which might change the curvature of the graphene layers. For the GO and GOS composite studied in the present case, this splitting is likely to be caused by the presence of the functional groups like epoxy, carbonyl, etc. Further, in the present study, for the SiO_2 decorated GO sheet, generally the G-band exhibits a shift towards lower wave number (from GO to GOS3) due to hybridization of GO sheets with the electron donor SiO_2. It has to be noted that such observation was also reported by Zhu *et al*.[36] in a study on GO enwrapped Ag/AgX composites.

The intensity ratio, I_D / I_G is a measure of the sp^3 disorder caused by functionalization and also due to the wrinkled morphology of GO. The increase in value of the I_D/ I_G ratio indicates the increase in disorder in the graphite material[37]. If we carefully examine the Raman spectra, when we go from GO to GOS3, the D-band shifts towards the lower wavenumber side, ie. from 1362 to 1350 cm^{-1} and the G2 peak shows similar red shift from 1614 to 1596 cm^{-1}. This indicates that while increasing the SiO_2 content, the composite system modified significantly and has well impact on its increase in disorder. Keeping above facts in mind, it is worthy to discuss the finding by Kou *et al*.[28] regarding the linkage between GO and SiO_2. According to them, silica particles non-covalently attached to carbon nanotubes, did not lead to any significant band shift or relative intensity variation within the Raman D-band. The increase of the D band relative intensity in the GOS system indicates that the silica particles are deposited on the surfaces of GO through some covalent linkage. The above mentioned things are more clear from the I_D/ I_G (by area) values, which increases from GO to GOS3 (1.19 to 2.20). This point can be further strengthened by the fact that the FWHM of the G1 and D-bands exhibits a broadening nature in our most of the cases while going from pure GO to

GOS with higher SiO_2 concentration. Thus, one can conclude that the spectral features of SiO_2 decorated GO sheets clearly exhibit a shift from sp^2 hybridization on carbon atoms to sp^3 while going from GO to GOS3, and also they are binded each other strongly.

Electrochemical characterization

The electrochemical biosensors function by the production and monitoring of current when a potential is applied between the two electrodes. In case of a second generation biosensors (mediated biosensors), the enzymes that can donate electrons to an electrochemically active electron acceptors. The efficiency and sensitivity of such biosensor can be greatly enhanced using a suitable mediator[38-39]. The Fe3+/2+ redox couple utilized here, exhibits a well-defined redox properties. It helps in the facile electron transfer arising from the biochemical reactions between the analyte (urea here) and enzymes (Urs-GLDH here), at a lower oxidation potentials.

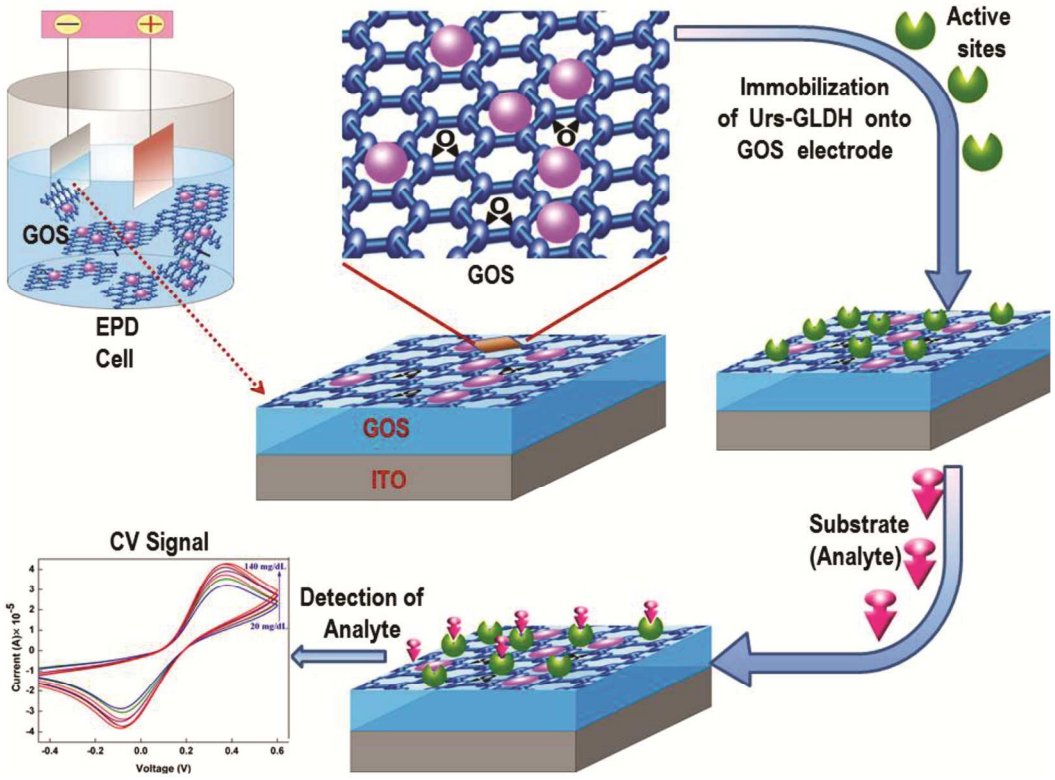

Figure 4. Shematic representation of electrochemical sensing set up for urea sensing.

Figure 4 shows a schematic representation of the electrochemical sensing set up used for urea sensing. This schematic sketch illustrates the procedure for the GOS electrode formation, immobilization with Urs-GLDH and detection of analytes using the CV technique.

Figure 5 (a) shows CV studies of ITO, GO/ITO, SiO_2/ITO, GOS/ITO and Urs-GLDH/GOS/ITO electrodes that have been conducted in PBS (pH= 7) containing 5mM $[Fe(CN)_6]^{3-/4-}$ using Autolab, Potentiostat/Galvanostat. The oxidation peak current of ITO is 46.2 µA, being reduced to 43.3 µA for GO due to the insulating nature of GO and it is further decreased to 39.4 µA for SiO_2. However, it has been observed that the current increases to 49 µA in the case of GOS/ITO electrode, indicating electrocatalytic activity of SiO_2 that result in improved electron transport property of GO. Resulting the high oxidation peak current among other electrodes fabricated, GOS taken as the working electrode for the present investigation on urea sensing. After the enzyme immobilization on GOS, the response current further decreases to 35.3 µA. The Urs-GLDH bienzyme has the macromolecular structure and the

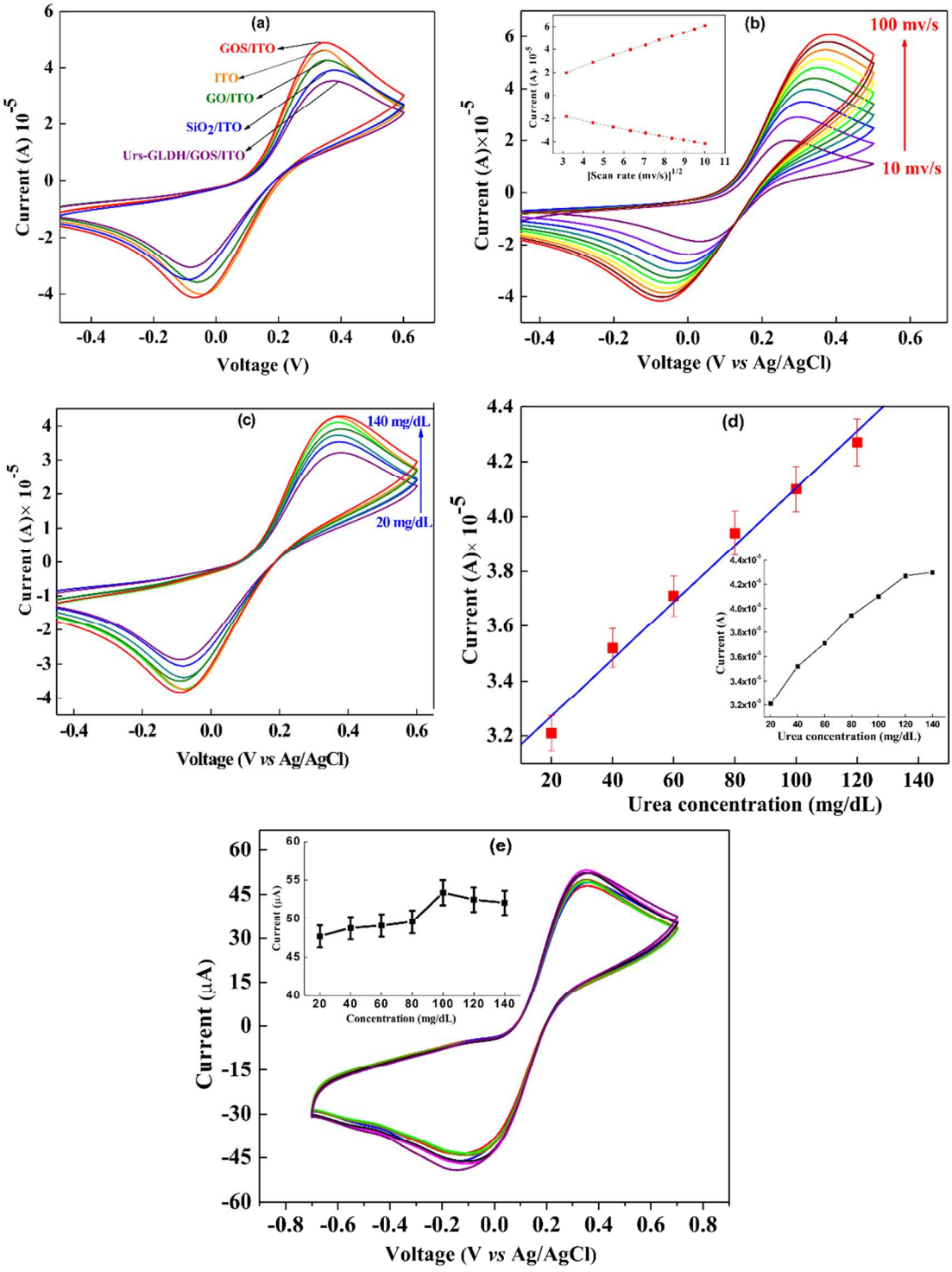

Figure 5. (a) CV of ITO, GO/ITO, SiO_2/ITO, GOS/ITO and Urs-GLDH/GOS/ITO electrodes, in PBS (pH= 7) containing 5mM $[Fe(CN)_6]^{3-/4-}$; **(b)**. CV of the Urs-GLDH/GOS/ITO bioelectrode at different scan rate (10 – 100 mV / s); (On inset: redox peak current as a function of square root of scan rate); **(c)**. Electrochemical response studies of the Urs-GLDH/GOS/ITO bioelectrode as a function of urea concentrations [20–140 mg/dL (3.3-23.2 mM)] using CV; **(d)**. Fitted calibration plot between anodic peak current and urea concentration (20-120 mg/dL); inset: calibration plot between anodic peak current and urea concentration (20-140 mg/dL); **(e)**. Control experiment of the GOS/ITO electrode as a function of urea concentration; inset: oxidation peak current vs. urea concentration plot of the GOS/ITO electrode.

redox active sites that are deeply embedded in this macromolecular structure. Besides this, the insulating characteristic of these enzymes results in reduced current. Furthermore because of the reduced conductivity of the Urs-GLDH/GOS/ITO bioelectrode, the oxidation peak potential shifts more towards a positive potential (0.371 V) as compared to that of the GOS/ITO electrode (0.347 V). Further, the peak separation between the oxidation and reduction peak currents obtained for GOS/ITO electrode (90.3 µA) has been found to be higher as compared to its counterparts GO/ITO (77.8 µA) and SiO_2/ITO (74µA). Figure 5 (b) shows CVs of the Urs-GLDH/GOS/ITO bioelectrode obtained as a function of the scan rate from 10 to100 mV/s. A proportional increase of the redox current with respect to the square root of the scan rate is observed, indicating a diffusion controlled system following *Eq. (1-2).*

$$I_a\,[A] = 2.1\times10^{-6}\,[A] + 5.9\times10^{-6}\,[A^2s/mV]^{1/2} \times \{\text{scan rate (mV/s)}\}^{1/2} \ldots. \text{(Eq.1)}$$

$$I_c\,[A] = -8.6\times10^{-6}\,[A] - 3.3\times10^{-6}\,[A^2s/mV]^{1/2} \times \{\text{scan rate (mV/s)}\}^{1/2} \ldots. \text{(Eq.2)}$$

The diffusion coefficient value (D) of the redox species for the Urs-GLDH/ GOS/ITO bioelectrode has been estimated from the slope of I_p versus $\nu^{1/2}$ plot using the Randel-Sevcik equation:

$$Ip = (2.69 \times 10^5)\, n^{3/2} A D^{1/2} C \nu^{1/2} \ldots\ldots\ldots\ldots\ldots\ldots \text{(Eq. 3)},$$

Where, I_p is the peak current (I_{pa} anodic and I_{pc}cathodic), n is electron stoichiometry, A is the electrode area (0.25 cm^2), D is the diffusion coefficient, C is the concentration of redox species (5 mM $[Fe(CN)^6]^{3-/4-}$) in mol/cm^3, and ν is the scan rate. The D value has been obtained as 3.6×10^{-7} cm^2 s^{-1}.

The electrochemical sensing studies of the Urs-GLDH/GOS/ITO bioelectrode have been carried out as a function of urea concentration in the presence of 30 µL of nicotinamide adenine dinucleotide (NADH,3.7 mg/dL) and 70 µL of α-Ketoglutarate (α-KG, 47.5 mg/dL) using cyclic voltammetry in PBS solution 50 mM PBS (pH 7, 0.9% NaCl) containing 5 mM $[Fe(CN)_6]^{3-/4-}$. It is observed that magnitude of the response current obtained for the Urs-GLDH/GOS/ITO bioelectrode increases as the concentration of urea increases (Figure 5(c)).

Figure 5(d) shows the linear calibration plot between anodic peak current and urea concentration (20-120 mg/dL). The response current varies proportionally as a function of urea concentration in this detection range.The calibration curve displayed in Fig. 5(d) has been fitted between the urea concentration and the value of anodic peak current that obeys Eq. 3.

$$I_a\text{(Urs-GLDH/GOS/ITO)}\,[A] = 3.06\times10^{-6}\,[A] + 1.04\times10^{-7} A/(mg/dL) \times \{\text{urea concentration (mg/dL)}..\text{(Eq.4)}$$

To the next higher value of urea concentration (140 mg/dL), there is no significant increase in response current and the Urs-GLDH/GOS/ITO bioelectrode is getting saturated there [inset of Figure 5(d)].

The lower detection limit for the GOS bioelectrode obtained as 2.1 mM using the 3σ/m criteria, where m is the slope and σ is standard deviation of the calibration graph. The linear range lies between 3.3-19.9 mM with a good sensitivity of 2.6μA/mM/cm^2.

Further, we have performed the control experiment using the GOS/ITO electrode as a function of urea concentration conducted in PBS containing 5 mM $[Fe(CN)_6]^{3-/4-}$ [(Figure 5(e)]. It has been observed that the response current obtained for GOS/ITO does not significantly change as a function of urea concentration [Inset, Figure 5(e)].

During the biochemical reaction (depicted in Figure 6), Urs catalyzes decomposition of urea into hydrogen bicarbonate (HCO_3^-) and ammonium (NH_4^+) ions. It has been found that ammonium ions simply diffuse into the solution. Thus, it is required to add GLDH as it catalyzes the reaction GLDH catalyzes the reversible reaction between α-KG and NH_3 to NAD+ and linked oxidative deamination of L-glutamate in two steps. The first step involves a Schiff base intermediate formed between NH3 and α-KG. Then Schiff base intermediate protonated due to transfer of the hydride ions from NADH resulting in formation of L-glutamate. NAD+ is utilized in the forward reaction of α-KG and free NH_3 that is converted to L-glutamate via hydride transfer from NADH to glutamate. NAD+ is utilized in the reverse reaction, involving L-glutamate being converted to α-KG and free (NH_3) via oxidative deamination reaction.[2,40,38] The electrons generated during these reactions are transferred to GOS/ITO electrode through a Fe (III)/Fe (IV) redox probe providing signal in the form of current.

The biochemical reaction is formulated below:

$$(NH_2)_2CO + 3H_2O \xrightarrow{Urs} NH_4^+ + OH^- + HCO_3^- \text{.....(Step A)}$$

$$NH_4^+ + \alpha\text{ - ketoglutarate} + NADH \xrightarrow{GLDH} \text{L-glutamate} + NAD^+ + 2e\text{.....(Step B)}$$

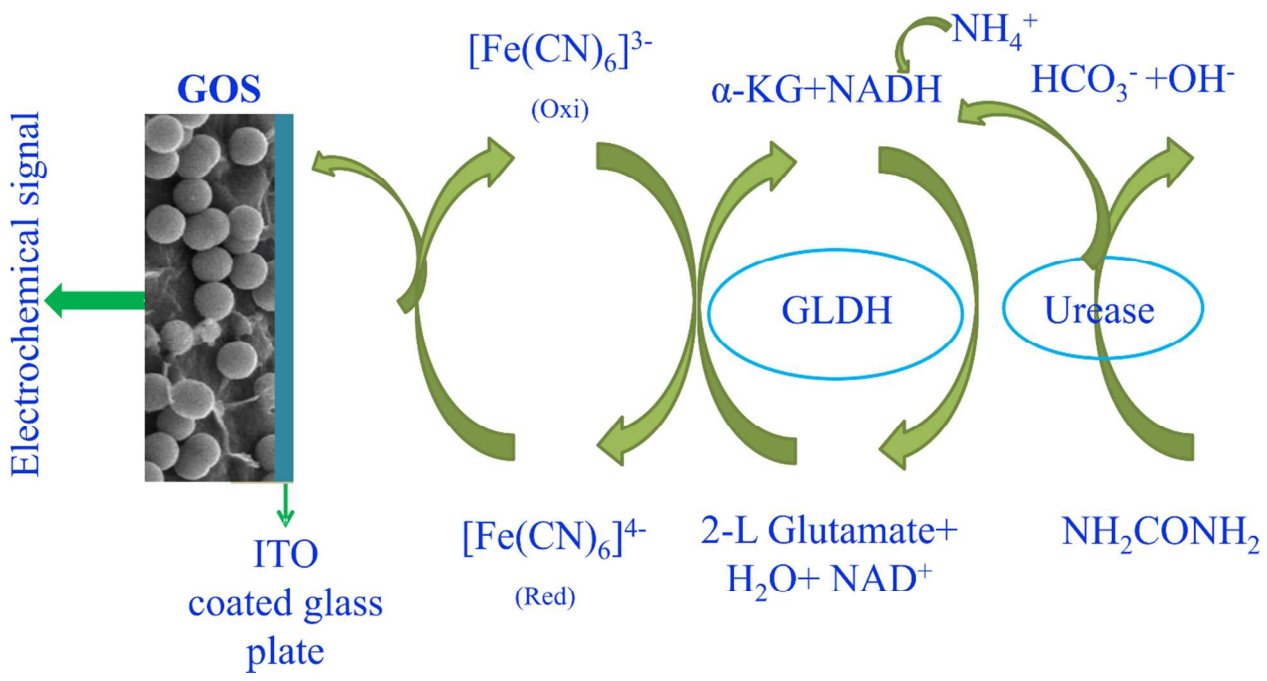

Figure 6. Schematic representation of electrochemical urea sensing mechanism using GOS bioelectrode.

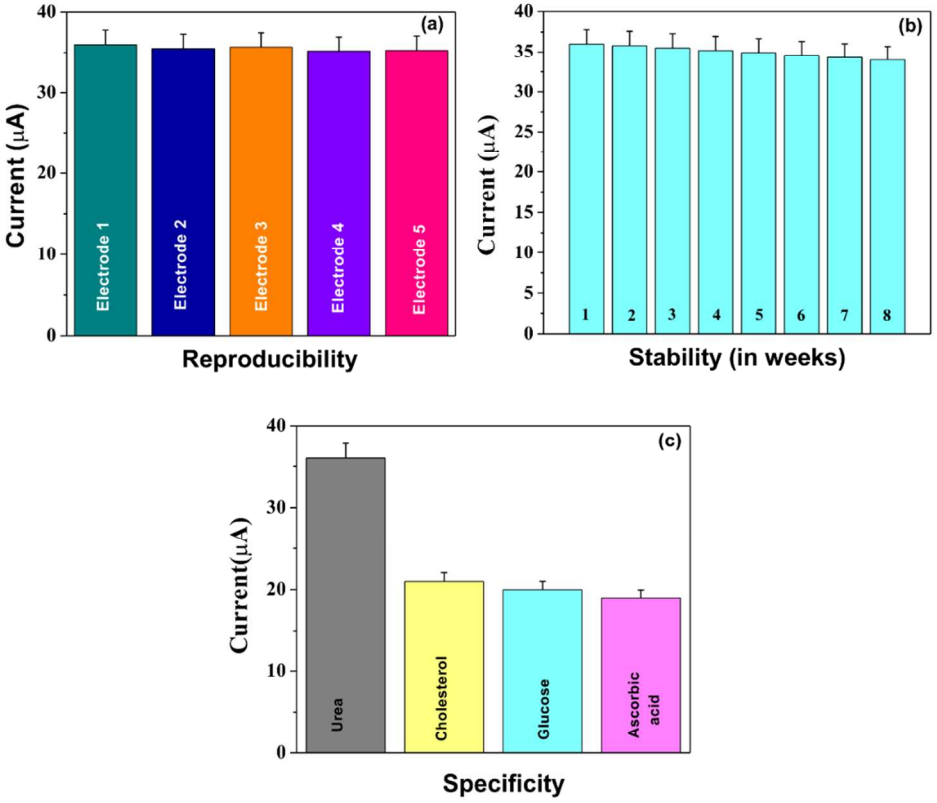

Figure 7. (a) Different Urs-GLDH/GOS/ITO bioelctrodes fabricated via the same condition applied to conduct the Reproducibility test; (b) Stability studies of Urs-GLDH/GOS/ITO bioelectrode measured at a regular interval one week upto eight weeks; (c) Specificity plot describing the CV response of Urs-GLDH/GOS/ITO bioelectrode in presence of urea, cholesterol, glucose and ascorbic acid.

The Urs-GLDH/GOS/ITO urea biosensor has been checked for its accountability by different tests such as reproducibility, specificity and stability measurements (Fig. 7). The reproducibility of Urs-GLDH/GOS/ITO bioelectrodes has been determined by monitoring the maximum peak current response for the five similar electrodes made under same protocol. It is found that, there is no major change in the peak current response (see the Fig. 7 a) and confirms the reproducibility of Urs-GLDH/GOS/ITO bioelectride as a reliable urea biosensor. The stability of the biosensor was monitored for a period of eight weeks at an interval of one week to see the peak current response change with respect to aging. There was only ~ 6 % decrease even after the eight weeks period when stored in refrigerated condition (4 °C) (Fig. 7 b). Further the Urs-GLDH/GOS/ITO urea biosensor's specificity towards urea has been measured to see the response with other analytes. For this, the interference monitored by checking the peak current response of Urs-GLDH/GOS/ITO in comparison with other interferants such as cholesterol, glucose and ascorbic acid. The absence of similar peak current response as like in case of urea is an indication of the high specificity of Urs-GLDH/GOS/ITO biosensor towards urea (Fig. 7c).

Table2. A comparative table describing the urea sensing characteristics of the bioelectrode -Urs-GLDH/GOS/ITO along with some other reported in literatures.

Bioelectrode	Detection Range(mM)	Detection Limit (mM)	Sensitivity	Stability (days)	Reff.
Urs-GLDH/GOS/ITO	3.3-19.9	2.1	2.6μA/mM/cm^2	35	Present work
Urs-GLDH/ZrO2/ITO	0.8–16.6	0.8	0.07 μA/mM/cm^2	-	[41]
MWCNT/silica	2.18×10^{-2}-1.07	-	2.3 mV/mM/cm^{-2}	60	[42]
Urs-GLDH/ZnO-Ch/ITO	0.8-16.6	0.49	0.13μA/mM/cm^2	90	[39]
Urs-PANi-nafion/Au	1-10	1	4.2μA/mM/cm^{-2}	-	[43]
Urs/PAPCP/ITO	0.16-5.02	-	0.47μA/mM/cm^2	60	[44]

The higher sensitivity obtained in our study as compared to the reported data (see Table 2) is due to excellent electrochemical properties and large surface area of GOS. Further, the mesoporous and biocompatable SiO_2 particles found to exhibit good electrocatalytic properties, which further enhance the response current as compared to GO. Moreover, the mesoporous morphology of SiO_2 particles facilitate surface density of enzyme loading. The faster response time (10 s) is attributed to rapid electron transfer kinetics of GO with abundant edge-plane defects.

Conclusions

SiO_2 particles of uniform size ~ 500 nm embedded on functional GO surface, which are quite useful for practical applications like biosensing, were synthesized and thoroughly characterized. The different techniques such as SEM, XRD were used for structural characterization, and for vibrational spectroscopy, IR and Raman were used. SEM images clearly revealed an almost uniform size of mesoporous SiO_2 particles evenly distributed on the GO sheets. Raman study of the GO and GOS composites clearly reveal that the degree of disorder increases from GO to GOS3. This indicates that during the formation of GOS composites, more sp^3 disorder is introduced into the sp^2 structure of graphene, i.e. the GO sheets get significantly modified. The IR spectra of both GO and GOS show that different functional groups, such as epoxy, alkoxy and carboxylic are attached to the GO sheet, which is manifested by the observation of several characteristic peaks of these functional groups. Owing to its different functional groups and optimum concentration, GOS3 showed high hydrophilicity, film forming capabilities and thereby good enzyme loading. The as synthesized GOS were electrophoretically deposited and biofunctionalized with urease (Urs) and glutamate dehydrogenase (GLDH) enzymes. The Urs-GLDH/ GOS/ITO bioelectrode has been utilized for the electrochemical biosensing of urea. The response studies of this urea sensor reveal high sensitivity of 2.6

μA/mM/cm^2, good detection limit of 2.1 mM and a well storage stability of 8 weeks. Further the reproducibility and specificity found to be well promising for the Urs-GLDH/ GOS/ITO bioelectrode to be used as an efficient urea biosensor. It should be interesting to utilize this easy and cost effective GO based platform, GOS for fabrication of other biosensors for application to clinical diagnostics.

Acknowledgements

The authors expresses there sincere gratitude to late. Prof. B. P. Asthana. The authors are also thankful to Dr. Andy Scheffel from IPHT, Jena for SEM measurements, Mrs. Anna Schmidt from IPC, Jena for BET measurements and Department of Applied Physics, I. I. T. (B. H. U.) for XRD measurements. Two of us (SA, JP) are thankful to Deutsche Forschungs-Gemeinschaft (DFG PO 563/15-1) for providing funds for the "Intensification of Bilateral Scientific Cooperation". AS acknowledges CAS program sponsored by UGC at Department of Physics, B. H. U. SA expresses his gratitude for the U.G.C. financial assistances and AvH fellowship.

References

1. K. S. Novoselov, A. K. Geim, S. V Morozov, D. Jiang, Y. Zhang, S. V Dubonos, I. V Grigorieva, and A. A. Firsov, *Sci.* , 2004, **306** , 666–669.

2. R. K. Srivastava, S. Srivastava, T. N. Narayanan, B. D. Mahlotra, R. Vajtai, P. M. Ajayan, and A. Srivastava, *ACS Nano*, 2011, **6**, 168–175.

3. M. Veerapandian, M.-H. Lee, K. Krishnamoorthy, and K. Yun, *Carbon N. Y.*, 2012, **50**, 4228–4238.

4. X. Liu, X. Xu, H. Zhu, and X. Yang, *Anal. Methods*, 2013, **5**, 2298–2304.

5. D. C. Marcano, D. V Kosynkin, J. M. Berlin, A. Sinitskii, Z. Sun, A. Slesarev, L. B. Alemany, W. Lu, and J. M. Tour, *ACS Nano*, 2010, **4**, 4806–14.

6. W. S. Hummers Jr and R. E. Offeman, *J. Am. Chem. Soc.*, 1958, **80**, 1339.

7. D. R. Dreyer, S. Park, C. W. Bielawski, and R. S. Ruoff, *Chem. Soc. Rev.*, 2010, **39**, 228–240.

8. Z. Wang, X. Zhou, J. Zhang, F. Boey, and H. Zhang, *J. Phys. Chem. C*, 2009, **113**, 14071–14075.

9. W. D. Pu, L. Zhang, and C. Z. Huang, *Anal. Methods*, 2012, **4**, 1662–1666.

10. T. Kuila, S. Bose, P. Khanra, A. K. Mishra, N. H. Kim, and J. H. Lee, *Biosens. Bioelectron.*, 2011, **26**, 4637–48.

11. M. Pumera, *Chem. Soc. Rev.*, 2010, **39**, 4146–4157.

12. A. M. V. Mohan, K. K. Aswini, A. M. Starvin, and V. M. Biju, *Anal. Methods*, 2013, **5**, 1764–1770.

13. W. Yang, K. R. Ratinac, S. P. Ringer, P. Thordarson, J. J. Gooding, and F. Braet, *Angew. Chemie Int. Ed.*, 2010, **49**, 2114–2138.

14. G. Goncalves, P. A. A. P. Marques, C. M. Granadeiro, H. I. S. Nogueira, M. K. Singh, and J. Gracio, *Chem. Mater.*, 2009, **21**, 4796–4802.

15. I. V Lightcap, T. H. Kosel, and P. V Kamat, *Nano Lett.*, 2010, **10**, 577–583.

16. S. Ge, M. Sun, W. Liu, S. Li, X. Wang, C. Chu, M. Yan, and J. Yu, *Sensors Actuators B Chem.*, 2014, **192**, 317–326.

17. A. F. de Faria, A. C. M. de Moraes, P. D. Marcato, D. S. T. Martinez, N. Durán, A. G. Souza Filho, A. Brandelli, and O. L. Alves, *J. Nanoparticle Res.*, 2014, **16**, 1–16.

18. Z. Luo, X. Ma, D. Yang, L. Yuwen, X. Zhu, L. Weng, and L. Wang, *Carbon N. Y.*, 2013, **57**, 470–476.

19. H. A. Ab Wab, K. A. Razak, and N. D. Zakaria, *J. Nanoparticle Res.*, 2014, **16**, 1–14.

20. B. G. Trewyn, S. Giri, I. I. Slowing, and V. S.-Y. Lin, *Chem. Commun.*, 2007, 3236–3245.

21. W. Stöber, A. Fink, and E. Bohn, *J. Colloid Interface Sci.*, 1968, **26**, 62–69.

22. M. Qhobosheane, S. Santra, P. Zhang, and W. Tan, *Analyst*, 2001, **126**, 1274–1278.

23. G. Tolnai, F. Csempesz, M. Kabai-Faix, E. Kálmán, Z. Keresztes, A. L. Kovács, J. J. Ramsden, and Z. Hórvölgyi, *Langmuir*, 2001, **17**, 2683–2687.

24. H.-H. Yang, S.-Q. Zhang, X.-L. Chen, Z.-X. Zhuang, J.-G. Xu, and X.-R. Wang, *Anal. Chem.*, 2004, **76**, 1316–1321.

25. J. Wang, *Anal. Chim. Acta*, 1999, **399**, 21–27.

26. W. Lu, Y. Luo, G. Chang, and X. Sun, *Biosens. Bioelectron.*, 2011, **26**, 4791–7.

27. S. Watcharotone, D. A. Dikin, S. Stankovich, R. Piner, I. Jung, G. H. B. Dommett, G. Evmenenko, S.-E. Wu, S.-F. Chen, and C.-P. Liu, *Nano Lett.*, 2007, **7**, 1888–1892.

28. L. Kou and C. Gao, *Nanoscale*, 2011, **3**, 519–528.

29. J. Liu, Q. Zhang, X. Chen, and J. Wang, *Chem. Eur. J.*, 2011, **17**, 4864–4870.

30. D. C. Marcano, D. V Kosynkin, J. M. Berlin, A. Sinitskii, Z. Sun, A. Slesarev, L. B. Alemany, W. Lu, and J. M. Tour, *ACS Nano*, 2010, **4**, 4806–4814.

31. J. Yan, T. Wei, B. Shao, F. Ma, Z. Fan, M. Zhang, C. Zheng, Y. Shang, W. Qian, and F. Wei, *Carbon N. Y.*, 2010, **48**, 1731–1737.

32. P. Innocenzi, P. Falcaro, D. Grosso, and F. Babonneau, *J. Phys. Chem. B*, 2003, **107**, 4711–4717.

33. R. M. Almeida and C. G. Pantano, *J. Appl. Phys.*, 1990, **68**, 4225–4232.

34. K. N. Kudin, B. Ozbas, H. C. Schniepp, R. K. Prud'Homme, I. A. Aksay, and R. Car, *Nano Lett.*, 2008, **8**, 36–41.

35. H. M. Heise, R. Kuckuk, A. K. Ojha, A. Srivastava, V. Srivastava, and B. P. Asthana, *J. Raman Spectrosc.*, 2009, **40**, 344–353.

36. M. Zhu, P. Chen, and M. Liu, *ACS Nano*, 2011, **5**, 4529–4536.

37. D. Graf, F. Molitor, K. Ensslin, C. Stampfer, A. Jungen, C. Hierold, and L. Wirtz, *Nano Lett.*, 2007, **7**, 238–242.

38. A. Chaubey and B. D. Malhotra, *Biosens. Bioelectron.*, 2002, **17**, 441–456.

39. P. R. Solanki, A. Kaushik, A. A. Ansari, G. Sumana, and B. D. Malhotra, *Appl. Phys. Lett.*, 2008, **93**, 163903.

40. M. A. Ali, S. Srivastava, P. R. Solanki, V. Reddy, V. V Agrawal, C. Kim, R. John, and B. D. Malhotra, *Sci. Rep.*, 2013, **3**.

41. G. Sumana, M. Das, S. Srivastava, and B. D. Malhotra, *Thin Solid Films*, 2010, **519**, 1187–1191.

42. T. Ahuja, D. Kumar, N. Singh, and A. M. Biradar, *Mater. Sci. Eng. C*, 2011, **31**, 90–94.

43. Y.-C. Luo and J.-S. Do, *Biosens. Bioelectron.*, 2004, **20**, 15–23.

44. V. Bisht, W. Takashima, and K. Kaneto, *Biomaterials*, 2005, **26**, 3683–3690.